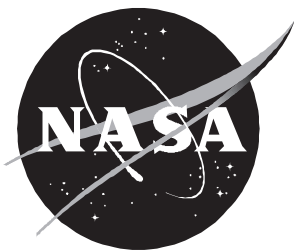




Multiple-Scattering Model for Inclusive Proton Production in Heavy Ion Collisions

Francis A. Cucinotta



Multiple-Scattering Model for Inclusive Proton Production in Heavy Ion Collisions

Francis A. Cucinotta
Langley Research Center • Hampton, Virginia

This publication is available from the following sources:

NASA Center for Aerospace Information
800 Elkridge Landing Road
Linthicum Heights, MD 21090-2934
(301) 621-0390

National Technical Information Service (NTIS)
5285 Port Royal Road
Springfield, VA 22161-2171
(703) 487-4650

Abstract

A formalism is developed for evaluating the momentum distribution for proton production in nuclear abrasion during heavy ion collisions using the Glauber multiple-scattering series. Several models for the one-body density matrix of nuclei are considered for performing numerical calculations. Calculations for the momentum distribution of protons in abrasion are compared with experimental data for inclusive proton production.

Introduction

The prediction of the secondary distribution of particles produced in heavy ion collisions is required for performing cosmic-ray transport calculations (ref. 1). The fragmentation cross sections in heavy ion reactions may be described in the abrasion-ablation models in which abrasion describes the knockout of nucleons and clusters during the projectile and target overlap and ablation describe the de-excitation of the projectile or target remnants. The abrasion cross sections are typically described using a geometric model (ref. 2) or semiclassical methods based on the Glauber or eikonal approximation (refs. 3-5).

In this report we consider the use of the Glauber multiple-scattering model for formulating the proton momentum distribution from abrasion. This formalism will be useful for obtaining both a better understanding of the physics of nuclear abrasion and estimates of secondary yields of light particles from direct processes. We will also relate the inclusive nucleon scattering observables to the internal nuclear density matrix that differs from the intranuclear cascade (ref. 6) or hydrodynamic model (ref. 7) descriptions of these observables. The calculations may then provide tests on nuclear structure calculations for the internal momentum distribution when all secondary nucleon mechanisms are considered. The same formalism describes proton or neutron production from nuclear abrasion; however, because of increased multiplicity for evaporation neutrons as compared with that of protons, we present calculations for proton production in this report.

Several mechanisms for proton (or neutron) production occur in heavy ion collisions. Figure 1 illustrates the mechanisms for proton production in nucleon-induced reactions. The contributions from the scattering of the incident nucleon from the target ground and low-lying excited states are close to the beam energy. Below the beam energy we find, first, the quasi-elastic peak where the projectile has knocked target nucleons into continuum states, and this is followed by the nucleon excitation peak which

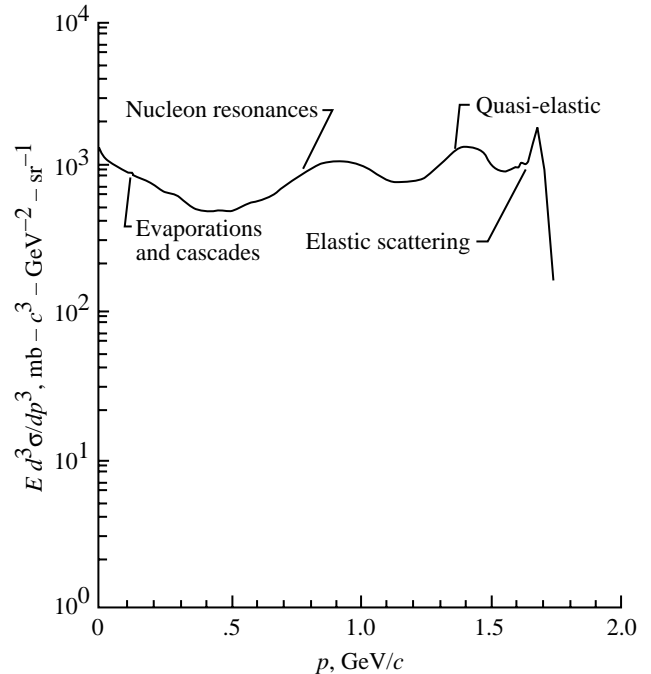


Figure 1. Schematic of mechanisms of proton production in nucleon-induced reactions.

at intermediate energies is dominated by the delta resonance. The nucleon excitation peak is observed to grow in importance with increasing beam energy and with the production angle of nucleons. For incident neutrons (protons), a quasi-elastic peak of protons (neutrons) is observed because of charge exchange. At lower energies, the two contributions to proton production are (1) the evaporated particles from the deexcitation of the target nucleus and (2) a higher energy contribution from the knockout or cascade particles and the multiple scattering of such particles inside the target. The cascade particles extend out to several hundred MeV because of the multiple scattering and the internal Fermi motion of the target, and these particles will overlap with the quasi-elastic peak at forward angles if the beam energy is not too high.

For heavy ion reactions, many of the same mechanisms will contribute to proton production however modified, because both the projectile and target nuclei are a source of evaporation and knockout protons. An illustration of the contributions to proton production in heavy ion collisions is shown in figure 2. The internal Fermi motion of the projectile allows secondary protons (or neutrons) to be produced at appreciably higher energies than the beam. The nucleon excitation peak will still appear in the intermediate region between the projectile and target. One important difference between the nucleon-induced and heavy-ion-induced proton production is the possibility of coherence effects which may lead to stronger multiple-scattering contributions for heavy ion reactions. In this report we will describe the calculation of proton spectra from the knockout mechanism. The contributions from nucleon excitation and evaporation will be described elsewhere.

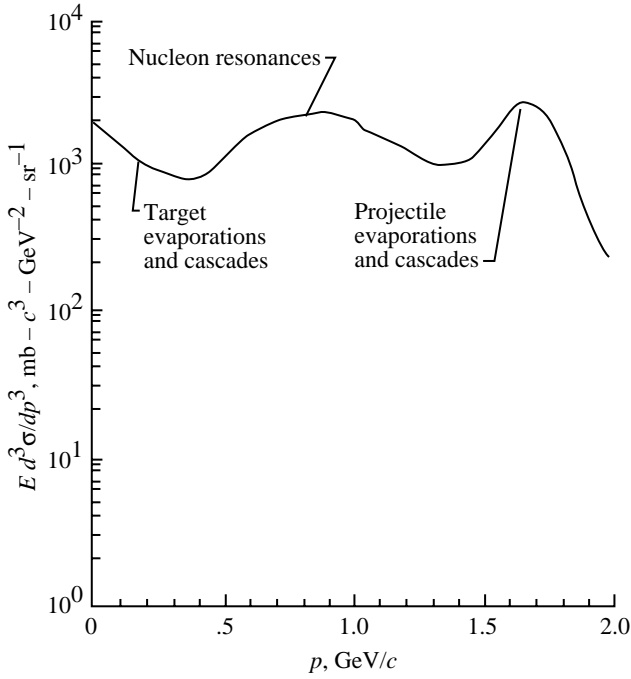


Figure 2. Schematic of mechanisms of proton production in heavy ion reactions.

Symbols

A	mass number	E	energy, MeV
b	impact parameter, fm	F	fragment
c	speed of light, m/sec	F^*	prefragment
		f	scattering amplitude, fm
		f_{NN}	nucleon-nucleon scattering amplitude
		Im	imaginary part of function
		K	initial wave number, fm^{-1}
		k	wave number of knockouts, fm^{-1}
		M	mass, MeV/c^2
		m_N	nucleon mass, MeV/c^2
		N_1	single-collision term
		n	number of abraded nucleons
		$n(p)$	momentum distribution
		P	projectile
		p	momentum, MeV/c
		Q	defined in equation (13)
		q	momentum transfer, fm^{-1}
		\mathbf{r}	internal nuclear coordinate vector
		S_n	separation energy, MeV
		\mathbf{s}	transverse part of \mathbf{r} vector
		T	target
		T_{F^*}	kinetic energy of prefragment, MeV
		t	time, sec
		X	final target state
		Γ	profile function
		δ	Dirac delta function
		Λ_n	defined in equation (20)
		ξ	defined in equation (22)
		$\rho(\mathbf{r}, \mathbf{r}')$	one-body density matrix, fm^{-3}
		$\rho(r)$	one-body density, fm^{-3}
		σ	cross section, mb
		χ	eikonal phase
		Ω	eikonal inelastic collision term

Abrasion Theory

In the Glauber model the scattering operator for nucleus-nucleus collisions is written as

$$f = \frac{iK}{2\pi} \int d^2b e^{i\mathbf{q}\cdot\mathbf{b}} \Gamma(\mathbf{b}) \quad (1)$$

(refs. 8 and 9) where K is the projectile-target relative wave number, b is the impact parameter, q is the momentum transfer, and the profile function representing the multiple-scattering series at high energies is

$$\Gamma(\mathbf{b}) = 1 - \prod_{\alpha,j} [1 - \Gamma_{\alpha j}(\mathbf{b} - \mathbf{s}_\alpha - \mathbf{s}_j)] \quad (2)$$

where α and j label the target and projectile constituents, respectively. In equation (2), $\Gamma_{\alpha j}$ is the two-body profile function with the internal coordinate having components $\mathbf{r} = (\mathbf{s}, z)$.

The scattering amplitude of equation (1) is related to the production cross section for a projectile nucleon from the abrasion process by

$$\begin{aligned} \frac{d\sigma}{d\mathbf{k}} &= \sum_X \frac{1}{(2\pi)^2} \int dE_{F^*} d^2q d^2b d^2b' e^{i\mathbf{q}\cdot(\mathbf{b}-\mathbf{b}')} \delta(E_i - E_f) \\ &\times \int \prod_{j=2}^n \left[\frac{d\mathbf{k}_j}{(2\pi)^3} \right] \langle TP | \Gamma^\dagger(\mathbf{b}') | XF^* \mathbf{k}_j \rangle \langle \mathbf{k}_j F^* X | \Gamma(\mathbf{b}) | PT \rangle \end{aligned} \quad (3)$$

where \mathbf{k}_j denotes the wave numbers of the abraded nucleons, F^* denotes the prefragment (with $A_{F^*} = A_P - n$), and we have inserted initial and final states in equation (3).

The state dependence of the final target energy prevents closure on these states from being automatic in equation (3), although when energy conservation is not considered it is made outright (ref. 3). If we consider the change in energy of the target from the collision

$$\begin{aligned} E_T - E_X &= E_T - \sqrt{(\mathbf{p}_T - \mathbf{q})^2 + M_X^2} \\ &= E_T \left(1 - \sqrt{1 + \frac{q^2 + M_X^2 - M_T^2}{E_T^2}} \right) \end{aligned} \quad (4)$$

where M_T and M_X are the mass of the target in the initial and final states, respectively, we expect that performing closure on $|X\rangle$ will be valid for sufficiently large values of E_T . In proceeding with closure on the final target states, we now write

$$\frac{d\sigma}{d\mathbf{k}} = \frac{1}{(2\pi)^2} \int dE_{F^*} d^2q d^2b d^2b' e^{i\mathbf{q}\cdot(\mathbf{b}-\mathbf{b}')} \sigma_n(\mathbf{b}, \mathbf{b}', \mathbf{k}, \mathbf{q}, E_{F^*}) \quad (5)$$

where we define

$$\begin{aligned} \sigma_n(\mathbf{b}, \mathbf{b}', \mathbf{k}_j, \mathbf{q}, E_{F^*}) &= \langle T | \left\{ \int \prod_{j=2}^n \left[\frac{d\mathbf{k}_j}{(2\pi)^3} \right] \delta(E_i - E_f) \right. \\ &\quad \left. \times \langle P | \Gamma^\dagger(\mathbf{b}') | F^* \mathbf{k}_j \rangle \langle \mathbf{k}_j F^* | \Gamma(\mathbf{b}) | P \rangle \right\} | T \rangle \end{aligned} \quad (6)$$

In order to consider the energy-conserving delta function in equation (6), we introduce the Fourier transform pair

$$\sigma_n(t) = \int dE e^{-iEt} \sigma_n(E) \quad (7)$$

and

$$\sigma_n(E) = \int \frac{dt}{2\pi} e^{iEt} \sigma_n(t) \quad (8)$$

In the projectile rest frame we have

$$E_i - E_f = S_n - T_{F^*} + E_T - E_X - \sum_{j=1}^n \frac{\mathbf{k}_j^2}{2m_N} \quad (9)$$

where S_n is the separation energy and T_{F^*} is the recoil energy of the prefragment, including any excitation energy of the prefragments. We next go into temporal space in order to consider the $d\mathbf{k}_j$ integrals in equation (6) and thus rewrite equation (9) as

$$E_i - E_f = \bar{E} - \sum_{j=2}^n \frac{\mathbf{k}_j^2}{2m_N} \quad (10)$$

From equations (6) and (7) by using equation (10), we find

$$\begin{aligned} \sigma_n(t) = \langle T | \left\{ \int \prod_{j=2}^n \left[\frac{d\mathbf{k}_j}{(2\pi)^3} \right] e^{-i \sum_j \frac{\mathbf{k}_j^2}{2m_N} t} \right. \\ \left. \times \langle P | \Gamma^\dagger(\mathbf{b}') | F^* \mathbf{k}_j \rangle \langle F^* \mathbf{k}_j | \Gamma(\mathbf{b}) | P \rangle \right\} | T \rangle \end{aligned} \quad (11)$$

In order to simplify equation (11), we first factor the profile function into projectile participant and spectator terms as

$$\Gamma(\mathbf{b}) = 1 - \prod_{l=n+1}^{A_P} Q_l(\mathbf{b} - \mathbf{s}_l) \prod_{j=1}^n Q_j(\mathbf{b} - \mathbf{s}_j) \quad (12)$$

where

$$Q_j = \prod_{\alpha=1}^{A_T} (1 - \Gamma_{\alpha j}) \quad (13)$$

In the abrasion model the orbits of the prefragments are assumed to be nearly the same as those of the projectile. This is consistent with the use of the impulse and frozen nucleus approximations at high energies. A completely factored form in the participant and spectator coordinates is assumed for the projectile wave function

$$|P\rangle = |F\rangle |\phi_n\rangle \quad (14)$$

where $|F\rangle$ and $|\phi_n\rangle$ are the wave functions of the core (spectators) and of the knockouts (spectations), respectively. The antisymmetrization is ignored in equation (14), which should be accurate if the mass of F is much larger than the knockouts. Antisymmetrization in the subsystems of $|F\rangle$ and $|\phi_n\rangle$ may still be included. By using plane-wave states for $|\mathbf{k}_j\rangle$ and substituting equations (12) and (14) into equation (11), we find that

$$\begin{aligned} \sigma_n(t) = \langle T | \left\{ \binom{A_P}{n} \langle F | \prod_l Q_l^\dagger(\mathbf{b}' - \mathbf{s}'_l) | F^* \rangle \langle F^* | \prod_l Q_l(\mathbf{b} - \mathbf{s}_l) | F \rangle \int d\mathbf{r}_1 d\mathbf{r}'_1 e^{i\mathbf{k}\cdot\mathbf{x}_1} Q_1^\dagger(\mathbf{b}' - \mathbf{s}'_1) Q(\mathbf{b} - \mathbf{s}_1) \right. \\ \left. \times \prod_{j=2}^n \left[\int \frac{d\mathbf{k}_j}{(2\pi)^3} d\mathbf{r}_j d\mathbf{r}'_j e^{i\mathbf{k}_j\cdot\mathbf{x}_j} e^{-ik_j^2 t/2m_N} Q_j^\dagger(\mathbf{b}' - \mathbf{s}'_j) Q_j(\mathbf{b} - \mathbf{s}_j) \right] \phi_n(\mathbf{r}_1, \dots, \mathbf{r}_n) \phi_n^\dagger(\mathbf{r}'_1, \dots, \mathbf{r}'_n) \right\} | T \rangle \end{aligned} \quad (15)$$

where $\mathbf{x}_j = \mathbf{r}_j - \mathbf{r}'_j$. Using the coherent approximation for the target wave function in the intermediate states and the independent particle model for the fragment wave function leads to

$$\sigma_n(t) = \binom{AP}{n} \mathcal{P}^{AP-n}(\mathbf{b}, \mathbf{b}') \Lambda_{n-1}(\mathbf{b}, \mathbf{b}', t) \frac{dN_1}{d\mathbf{k}} \quad (16)$$

where the function $\mathcal{P}(\mathbf{b}, \mathbf{b}')$ describes the projectile spectators as given by

$$\mathcal{P}^{AP-n}(\mathbf{b}, \mathbf{b}') = \langle TF | \prod_l Q_l^\dagger(\mathbf{b}' - \mathbf{s}'_l) | F^* \rangle \langle F^* | \prod_l Q_l(\mathbf{b} - \mathbf{s}_l) | FT \rangle \quad (17)$$

We next perform closure on the prefragment states in equation (17) because we do not consider coincidences with individual states. After closure we find that

$$\mathcal{P}^{AP}(\mathbf{b}, \mathbf{b}') = \langle TF | \prod_l Q_l^\dagger(\mathbf{b}' - \mathbf{s}_l) Q_l(\mathbf{b} - \mathbf{s}_l) | FT \rangle \quad (18)$$

In equation (16) we have defined

$$\frac{dN_1}{d\mathbf{k}} = \frac{1}{(2\pi)^3} \int d\mathbf{r} d\mathbf{r}' e^{i\mathbf{k}\cdot\mathbf{x}} \rho(\mathbf{r}, \mathbf{r}') Q_l^\dagger(\mathbf{b}' - \mathbf{s}') Q_l(\mathbf{b} - \mathbf{s}) \quad (19)$$

where $\rho(\mathbf{r}, \mathbf{r}')$ is the one-body density matrix of the projectile given by $\rho(\mathbf{r}, \mathbf{r}') = \phi(\mathbf{r}) \phi^\dagger(\mathbf{r}')$. Next, from equation (15), after evaluation of the integrals over \mathbf{k}_j for $j > 2$, we find

$$\begin{aligned} \Lambda_{n-1}(\mathbf{b}, \mathbf{b}', t) &= \langle T | \int \prod_{j=2}^n \left[d\mathbf{r}_j d\mathbf{r}'_j \left(\frac{m_N}{2\pi i t} \right)^{3/2} e^{-m_N x_j^2 / 2it} \rho(\mathbf{r}_j, \mathbf{r}'_j) \right. \\ &\quad \left. \times Q_j(\mathbf{b}' - \mathbf{s}'_j) Q_j(\mathbf{b} - \mathbf{s}_j) \right] | T \rangle \end{aligned} \quad (20)$$

In energy space,

$$\begin{aligned} \Lambda_{n-1}(\mathbf{b}, \mathbf{b}', T_{F^*}, \mathbf{k}) &= \langle T | \int \prod_{j=2}^n \left[d\mathbf{r}_j d\mathbf{r}'_j \rho(\mathbf{r}_j, \mathbf{r}'_j) Q_j^\dagger(\mathbf{b}' - \mathbf{s}'_j) Q_j(\mathbf{b} - \mathbf{s}_j) \right] \\ &\quad \times \frac{m_N}{2} \left(\frac{1}{2\pi} \right)^{3(n-1)/2} \frac{\xi_{n-1}^{[3(n-1)/2]-1}}{\bar{x}_{n-1}^{[3(n-1)/2]-1}} J_{[3(n-1)/2]-1}^{(1)}(\xi_{n-1} x_{n-1}) | T \rangle \end{aligned} \quad (21)$$

where $J_m^{(1)}$ is the cylindrical Bessel function of the first kind of order m and where

$$\xi_{n-1} = \sqrt{2m_N \left[T_{F^*} + \frac{\mathbf{k}^2}{2m_N} - S_n - (E_T - E_X) \right]} \quad (22)$$

and

$$\bar{x}_{n-1} = \sqrt{\sum_{j=2}^n x_j^2} \quad (23)$$

For $n = 1$, we have $\Lambda_0 = \delta(T_{F^*})$. If we assume forward-peaked density matrices (about $\bar{x} = 0$), a small argument expansion of the Bessel functions can be developed (refs. 10 and 11) that results in

$$\begin{aligned} \Lambda_{n-1}(\mathbf{b}, \mathbf{b}', T_{F^*}, \mathbf{k}) &\approx C_{n-1} \left[T_{F^*} + \frac{\mathbf{k}^2}{2m_N} - S_n - (E_T - E_X) \right]^{n-1} \\ &\times \Lambda_1^{n-1} \left(\mathbf{b}, \mathbf{b}', \frac{\xi_{n-1}}{\sqrt{n-1}} \right) + O(\xi^4 x^4) \end{aligned} \quad (24)$$

where, for example, $C_1 = 1$, $C_2 = \pi/4$, $C_3 = \pi/105$, and $C_4 = \pi^2/240$.

The nucleon momentum distribution from abrasion then takes the form

$$\begin{aligned} \frac{d\sigma}{d\mathbf{k}} &= \sum_n \binom{A_P}{n} \frac{1}{(2\pi)^2} \int d^2q d^2b d^2b' e^{i\mathbf{q}\cdot(\mathbf{b}-\mathbf{b}')} \mathcal{P}^{A_P-n}(\mathbf{b}, \mathbf{b}') \\ &\times \frac{dN_1}{d\mathbf{k}} \int dT_{F^*} \Lambda_{n-1}(\mathbf{b}, \mathbf{b}', T_{F^*}, \mathbf{k}) \end{aligned} \quad (25)$$

If

$$q^2 + M_T^2 - M_X^2 \ll E_T^2 \quad (26)$$

we may approximate equation (25) as

$$\frac{d\sigma}{d\mathbf{k}} \approx \sum_n \binom{A_P}{n} \int d^2b \mathcal{P}^{A_P-n}(\mathbf{b}) \frac{dN_1}{d\mathbf{k}} \int dT_{F^*} \Lambda_{n-1}(\mathbf{b}, T_{F^*}, \mathbf{k}) \quad (27)$$

The result of equation (27) suggests that for $A_P \gg 1$, the momentum dependence of higher production terms ($n > 1$) should be similar to the leading-order terms as described in the appendix. This supports the success of the hard-scattering model of Hatch and Koonin (ref. 12) where only the single-scattering mechanism was used to predict the shape of the inclusive proton distribution in heavy ion collisions. The model developed herein differs from the hard-scattering model by our use of the target closure approximation in which the effects of smearing of the secondary momentum from the target knockouts are not considered but are replaced by averages represented by the target density and by using only on-shell two-body amplitudes. Also, the Glauber model has a much fuller multiple-scattering structure than the hard-scattering model.

In order to include the effects of final-state interactions (FSI) of the nucleon knockouts, we use the eikonal model described in reference 11 in which the plane waves are replaced by the distorted waves for the nucleon-projectile recoil interaction evaluated at the relative energy between the knockout and recoil. Modifying equation (19) as in reference 11 gives

$$\frac{dN_1}{d\mathbf{k}} = \frac{1}{(2\pi)^3} \int d\mathbf{r} d\mathbf{r}' e^{i\mathbf{k}\cdot\mathbf{x}} \rho(\mathbf{r}, \mathbf{r}') e^{-2\text{Im}\chi^{(-)}(y)} Q_l^\dagger(\mathbf{b}' - \mathbf{s}') Q_l(\mathbf{b} - \mathbf{s}) \quad (28)$$

where $\chi^{(-)}$ is the outgoing eikonal phase. Equation (28) ignores off-shell effects, whereas the energy dependence of the FSI is included and a medium modified interaction is assumed as described in reference 11.

Optical Limit for Profile Functions

For $A_P A_T \gg 1$, the optical limit of the profile functions occurring in the previous expressions may be used (refs. 8 and 13). From reference 13 we find in the optical limit that

$$\mathcal{P}^{A_P}(\mathbf{b}, \mathbf{b}') = \exp\left\{i\left[\chi(\mathbf{b}) - \chi^\dagger(\mathbf{b}')\right]\right\} \quad (29)$$

where the eikonal phase is

$$\chi(\mathbf{b}) = \frac{A_P A_T}{2\pi k_{\text{NN}}} \int d^2q e^{i\mathbf{q}\cdot\mathbf{b}} F_P(q) F_T(q) f_{\text{NN}}(q) \quad (30)$$

with F denoting the one-body form factor and f_{NN} denoting the two-body scattering amplitude, which we represent by

$$f_{\text{NN}} = \frac{\sigma_{\text{NN}}(\alpha + i) k_{\text{NN}}}{4\pi} e^{-\frac{1}{2}Bq^2} \quad (31)$$

where σ_{NN} is the two-body total cross section, B is the two-body slope parameter, and α is the ratio of the real part to the imaginary part of $f_{\text{NN}}(\mathbf{q} = 0)$. For the inelastic terms, we write in the optical limit (ref. 13)

$$Q_j^\dagger(\mathbf{b}' - \mathbf{s}'_j) Q_j(\mathbf{b} - \mathbf{s}_j) = \left\{ \exp\left[\tilde{\Omega}(\mathbf{b}' - \mathbf{s}'_j, \mathbf{b} - \mathbf{s}_j)\right] - 1 \right\} \quad (32)$$

with

$$\tilde{\Omega}(\mathbf{b}' - \mathbf{s}'_j, \mathbf{b} - \mathbf{s}_j) = \frac{1}{(2\pi k_{\text{NN}})^2} \sum_{\alpha} \int d^2q d^2q' e^{i\mathbf{q}\cdot(\mathbf{b}-\mathbf{s}_j+\mathbf{s}_\alpha)} e^{-i\mathbf{q}\cdot(\mathbf{b}'-\mathbf{s}'_j+\mathbf{s}'_\alpha)} f_{\text{NN}}(\mathbf{q}) f_{\text{NN}}^\dagger(\mathbf{q}') \quad (33)$$

Model for Nuclear Density Matrix

We next describe a local density approximation for the one-body density matrix. For a projectile nucleus with A_P nucleons, the one-body density matrix is defined in terms of the complete nuclear wave function (Ψ) as (ref. 14)

$$\rho(\mathbf{r}, \mathbf{r}') = \int d\mathbf{r}_2 d\mathbf{r}_3, \dots, d\mathbf{r}_{A_P} \Psi^\dagger(\mathbf{r}', \mathbf{r}_2, \dots, \mathbf{r}_{A_P}) \Psi(\mathbf{r}, \mathbf{r}_2, \dots, \mathbf{r}_{A_P}) \quad (34)$$

The evaluation of equation (34) requires knowledge of the complete nuclear wave function; however, in practice a model is introduced. In the Fermi gas model (ref. 14),

$$\rho(\mathbf{r}, \mathbf{r}') = \rho_o \frac{3j_1(k_F |\mathbf{r} - \mathbf{r}'|)}{k_F |\mathbf{r} - \mathbf{r}'|} \quad (35)$$

where k_F is the Fermi momentum and ρ_o is the density of nuclear matter. The Fermi gas model is known to provide a poor representation of the density matrix; however, its form suggests the use of a local density model where the density matrix factors are given as

$$\rho(\mathbf{r}, \mathbf{r}') \approx \rho(\mathbf{y}) n(\mathbf{x}) \quad (36)$$

with $\mathbf{x} = \mathbf{r} - \mathbf{r}'$ and $\mathbf{y} = \frac{1}{2}(\mathbf{r} + \mathbf{r}')$, and where the one-body density is given by the diagonal part of the density matrix

$$\rho(\mathbf{r}) = \rho(\mathbf{r}, \mathbf{r}' = \mathbf{r}) \quad (37)$$

Here, $n(\mathbf{x})$ is the Fourier transform of the nucleon momentum distribution

$$n(\mathbf{x}) = \int d\mathbf{p} e^{i\mathbf{p}\cdot\mathbf{x}} n(\mathbf{p}) \quad (38)$$

where $n(\mathbf{p})$ is defined by

$$n(\mathbf{p}) = \int d\mathbf{r} d\mathbf{r}' e^{i\mathbf{p}\cdot\mathbf{x}} \rho(\mathbf{r}, \mathbf{r}') \quad (39)$$

with normalization

$$\int n(\mathbf{p}) \frac{d\mathbf{p}}{(2\pi)^3} = 1 \quad (40)$$

The one-body density is reasonably well known from elastic electron scattering. The nucleon momentum distribution at small to modest values of p is known from inclusive inelastic electron scattering. For large values of p , the backward production of protons suggests that large enhancements occur because of correlation

effects in contrast to predictions of single-particle models and that the enhancements are largely independent of the nuclear mass (refs. 15–17). Before introducing phenomenological parameterizations of $n(\mathbf{p})$, we note that by using equations (36) and (33), equation (19) can be written as

$$\frac{dN_1}{d\mathbf{k}} = \frac{1}{(2\pi)^2} \int d^2x d^2p e^{i(\mathbf{k}_\perp - \mathbf{p}_\perp) \cdot \mathbf{x}_\perp} n\left(\sqrt{p_\perp^2 + k_L^2}\right) \times \int d^2y \rho(\mathbf{y}) \left[e^{\Omega(\mathbf{b}, \mathbf{x}, \mathbf{y})} - 1 \right] \quad (41)$$

where \mathbf{k}_\perp is the transverse part of \mathbf{k} and k_L is the longitudinal part of \mathbf{k}_0 . Equation (41) shows that the production spectrum in the longitudinal direction corresponds closely to the internal momentum distribution independent of the collision dynamics in the Glauber model, whereas the transverse spectrum is modified by multiple scattering.

Haneishi and Fujita (ref. 17) have introduced

$$n(\mathbf{p}) = n_0 \sum_{i=1}^3 C_i e^{-p^2/2p_i^2} \quad (42)$$

where C_i and p_i are constants listed in table 1. The last term in equation (42) is expected to directly reflect the nuclear correlations. In equation (42), p_1 is related to the Fermi momentum by $p_1 = \sqrt{2/5}k_F$. Values for k_F from experiments of Moins et al. (ref. 18) are listed in table 2. For ^{12}C we use a value for k_F corresponding to the matter radius of 1.69 fm.

Table 1. Parameters for Momentum Distribution Model of Equation (42)

i	p_i , MeV/ c	C_i
1	$\sqrt{2/5}k_F$	1
2	$\sqrt{6/5}k_F$	0.03
3	500	0.003 (0.0002) ^a

^aValue found empirically.

Table 2. Experimental Determination of Fermi Momentum for Several Nuclei

Nucleus	k_F , MeV/ c
^{12}C	184
^{40}Ar	251
^{208}Pb	265

Amado (ref. 19) has considered many body correlations by solving the Schrödinger equation directly for the case of delta-function potentials where, for large values of p , he finds

$$n(p) \approx \frac{\gamma p}{\sinh(\gamma p)} \quad (43)$$

An analysis of backward proton scattering supports the value $\gamma = 90$ MeV/ c independent of the nuclear mass. We continue equation (43) to small values of p by using

$$n(p) = n_0 \left[e^{-p^2/2p_1^2} + d_0 \frac{\gamma p}{\sinh(\gamma p)} \right] \quad (44)$$

and consider several values for d_0 below. We note that the normalization in equation (44) is given as

$$n_0 = \left[(2\pi p_1^2)^{3/2} + \frac{d_0 \pi^5 \gamma^3}{2} \right]^{-1} (2\pi)^3 \quad (45)$$

and for $n(\mathbf{x})$ we find that

$$n(\mathbf{x}) = n_0 \left[(2\pi p_1^2)^{3/2} e^{-p_1^2 x^2/2} + \frac{\pi^4 \gamma^2 d_0}{x} \operatorname{sech}^2\left(\frac{\pi \gamma x}{2}\right) \tanh\left(\frac{\pi \gamma x}{2}\right) \right] \quad (46)$$

In figures 3, 4, and 5, we compare the models of equations (42) and (44) for ^{12}C , ^{40}Ar , and ^{208}Pb , respectively. For display, $n(\mathbf{p})$ has been normalized to unity rather than to the condition given by equation (40). For a pure

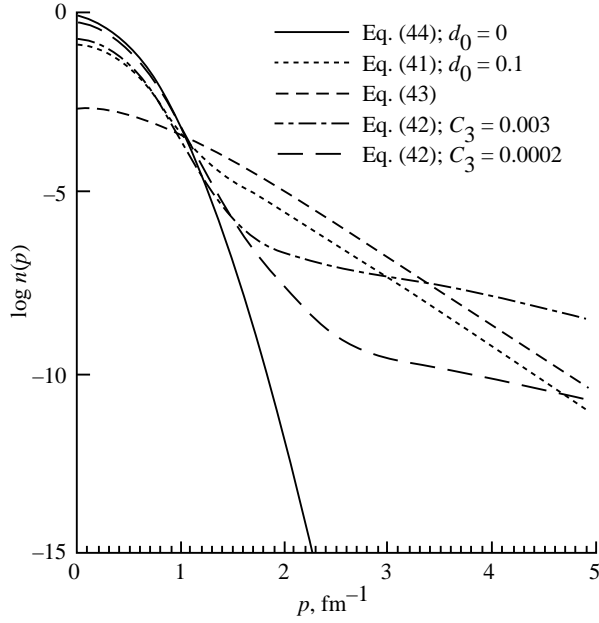


Figure 3. Logarithm of internal momentum distribution for ^{12}C versus momentum for several models.

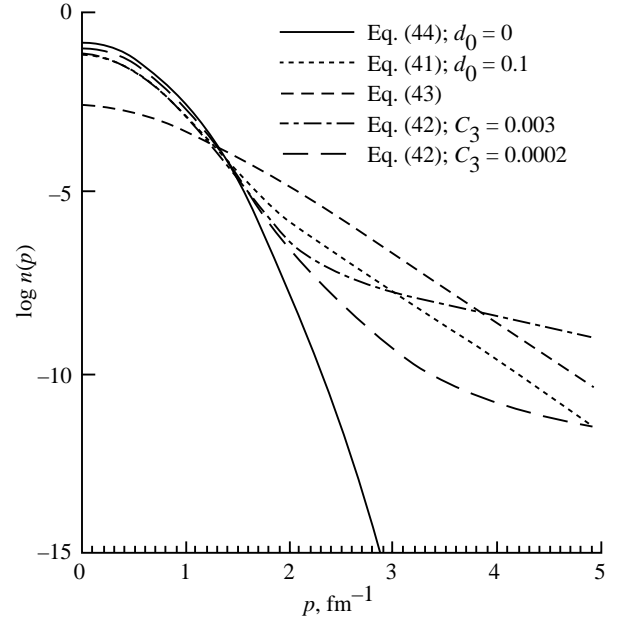


Figure 4. Logarithm of internal momentum distribution for ^{40}Ar versus momentum for several models.

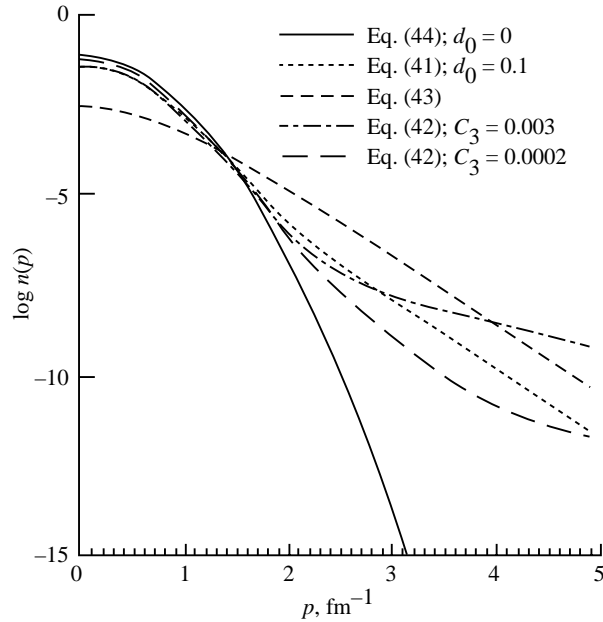


Figure 5. Logarithm of internal momentum distribution for ^{208}Pb versus momentum for several models.

Gaussian model ($d_0 = 0$ in eq. (44)), the momentum distribution is vanishingly small above about 3 fm^{-1} . The model of equation (42) is shown using $C_3 = 0.003$ and a value of $C_3 = 0.0002$ determined empirically, as discussed below. Including the correlation term with no Gaussian component (dashed line) is seen to show a large depletion of strength at small values of p in order to preserve the normalization condition. The use of equation (44) with $0.01 < d_0 < 0.1$ will provide a reasonable momentum distribution at small values of p and account for some correlation strength at large values of p .

Results and Discussion

In figure 6 we show calculations for the momentum distribution of produced protons in ^{12}C on ^{12}C reactions at an energy of $1.028A \text{ GeV}$ in the forward direction. The first three terms in the series of equation (25) are shown corrected for the production of protons only with the final-state interactions (FSI) neglected. The invariant momentum distribution is shown which is found by multiplying equation (25) by the energy of the secondary proton. The calculations are made by neglecting the correlation term (the third term) in equation (42). The leading-order term is seen to dominate, but with important contributions from the higher terms. The shape of the distribution for the higher order terms is similar to the leading term except at high momentum values where they fall off more rapidly. In figure 7 we compare calculations which include the final-state interactions

using the same internal momentum distribution as in figure 6. The absorptive effect of the FSI leads to a decrease of about a factor of 2 in the momentum distribution. This large decrease indicates the importance of cascade effects of the knockouts with the projectile fragments which must account for the decrease in figure 7.

In figure 8 we compare calculations for proton production from abrasion for several targets with the experimental data from references 20 and 21 for inclusive proton production. The calculations shown by the solid line include the correlation contribution in equation (42). However, the strength has been adjusted to $C_3 = 0.0002$ from the suggested value of $C_3 = 0.003$ from Haneishi and Fujita (ref. 17) because their value was found to be much too large in the high-momentum region. The dashed lines in figure 8 neglect the correlation term ($d_0 = 0$). A

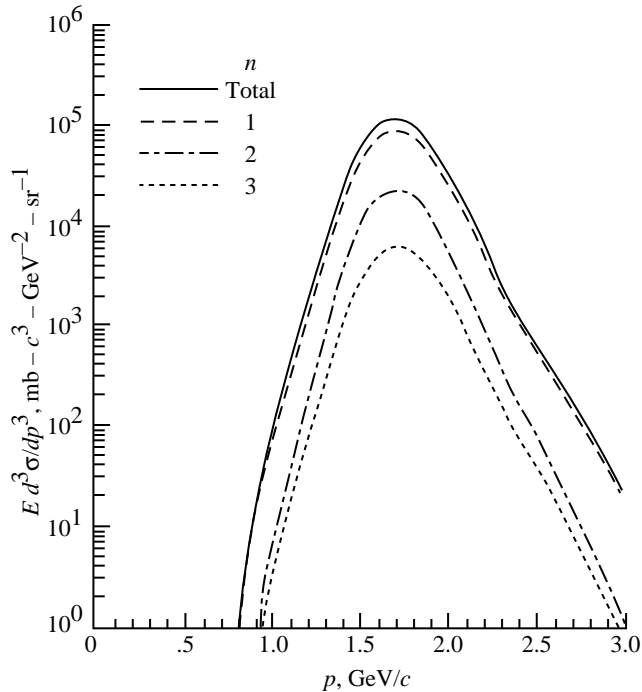


Figure 6. Calculations of invariant momentum distribution for proton production from abrasion in ^{12}C - ^{12}C collisions at $1.028A \text{ GeV}$. Shown are first three collision terms without final-state interactions.

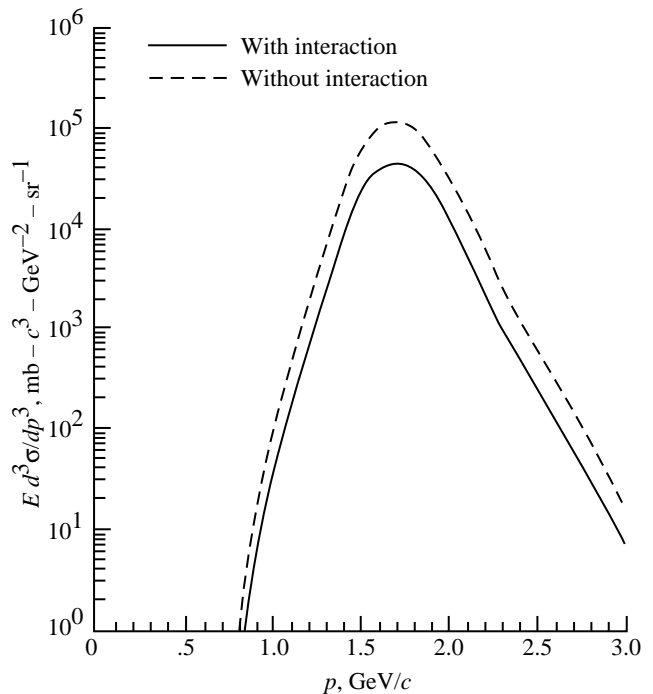


Figure 7. Calculations of invariant momentum distribution for proton production from abrasion in ^{12}C - ^{12}C collisions at $1.028A \text{ GeV}$ with and without final-state interactions.

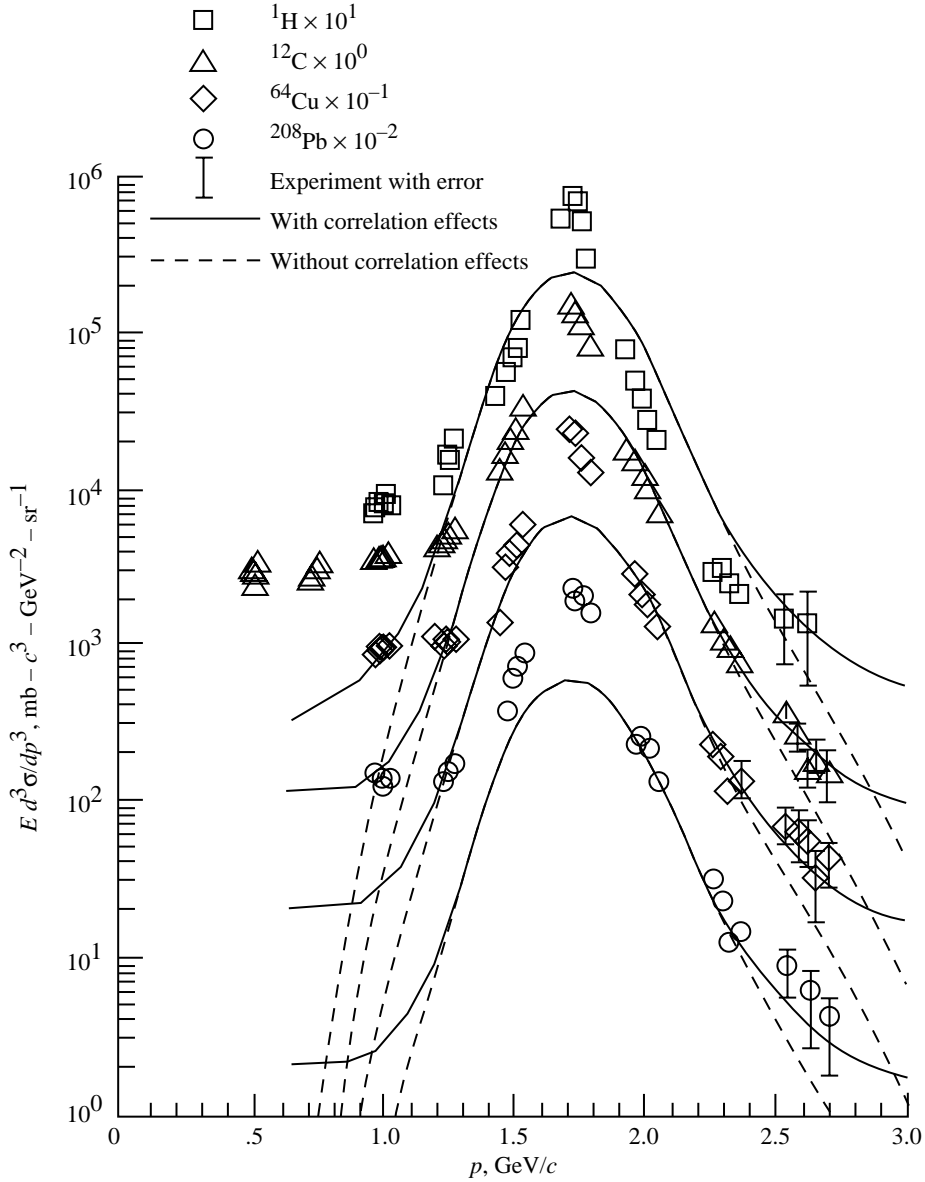


Figure 8. Comparison of calculations with experiments of references 20 and 21 for proton production for ^{12}C collisions on several target nuclei at 1.028A GeV. Calculations include final-state interactions with and without correlation effects as described in text.

treatment of phase space that is more accurate than the Glauber model employed here may allow for a larger correlation term; however, we note that most of the cited calculations on backwards proton production (refs. 15–17) neglect the absorptive effects that would cause some renormalization of their results. The agreement between calculations and experiments in figure 8 is fairly good except in the low-momentum region where other processes will contribute to the inclusive proton production. The calculations shown include the production from the target knockouts, but these make only a small contribution at large momenta. The largest differences in the high-momentum region occur for the ^1H tar-

get where we note that the experimental results are obtained indirectly by using a CH_2 target.

In figure 9 we compare calculations with experiments for proton production in ^{12}C – ^{12}C reactions at 2.062A GeV. The agreement between calculations is also good as in the lower energy data for the ^{12}C projectiles. In figure 10 we repeat the comparison made in figure 9 shown in the rest frame of the projectile. Also shown for comparison are plots of the internal momentum distribution times the proton energy normalized to the data. The comparison made in figure 10 illustrates the modification of the momentum distribution by the collision dynamics.

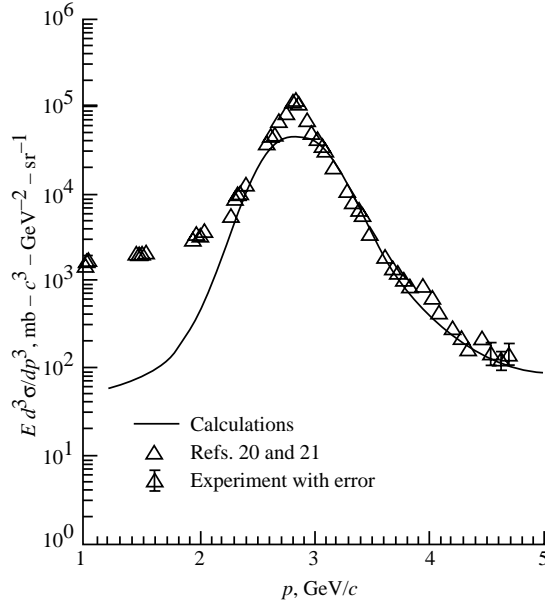


Figure 9. Comparison of calculations with experiments of references 20 and 21 for proton production in $^{12}\text{C}-^{12}\text{C}$ collisions at 2.062A GeV.

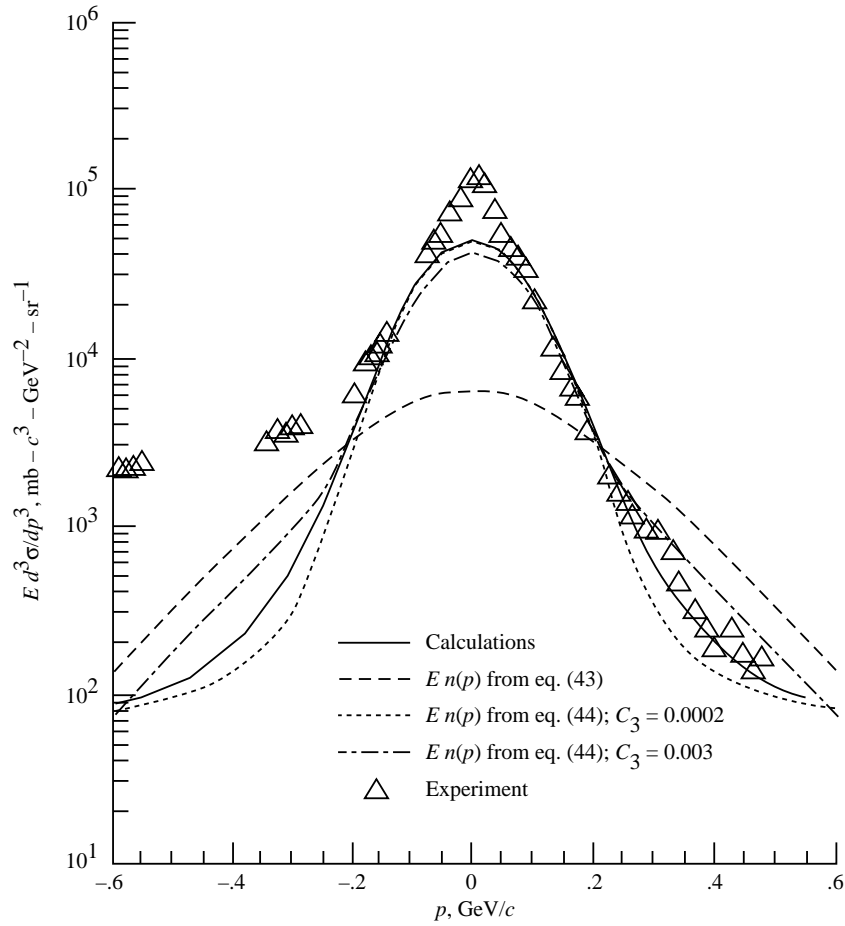


Figure 10. Comparison of calculations with experiments of references 20 and 21 for proton production in $^{12}\text{C}-^{12}\text{C}$ collisions at 2.062A GeV in projectile rest frame. Also shown is plot of $E n(p)$ for models discussed in test.

In figure 11 we show calculations of proton production in Ar–KCl collisions at 0.8A GeV at a scattering angle of 10° in comparison with the data of Nagamiya et al. (ref. 22). For calculations, the target is assumed to be Ar, and the agreement is again good in the high-momentum region. At low values of momentum, other contributions to the inclusive proton production, as discussed in the introduction of this report, are present and have not been estimated here. Production mechanisms other than those from abrasion will become more dominant at larger scattering angles. Finally, in figure 12 we show comparisons with the data of reference 23¹ for proton production at 5° from ⁴⁰Ar projectiles interacting with Be and Cu targets.

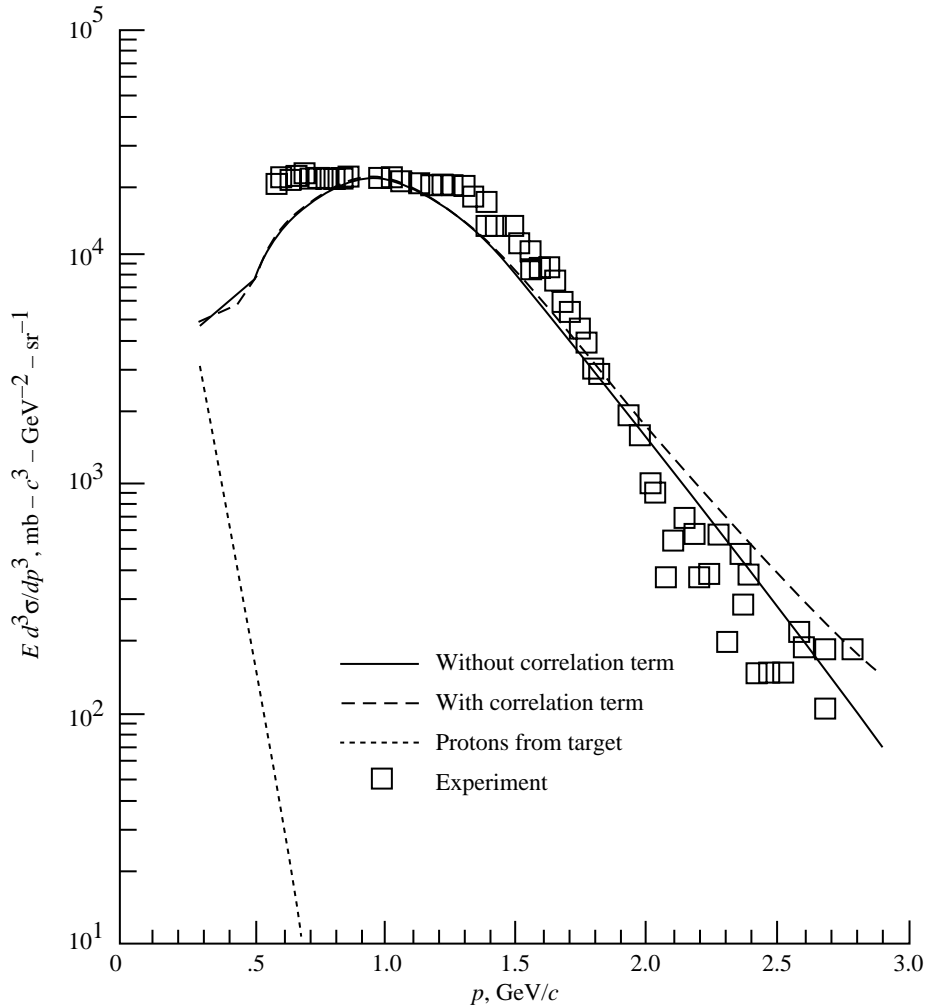


Figure 11. Comparison of calculations with experiments of reference 22 for proton production at 10° in ⁴⁰Ar–⁴⁰Ar collisions at 0.8A GeV. Data are for Ar–KCl and show calculations both with and without correlation term and protons from target.

¹A vital comparison was also made with data found in an unpublished report by V. Perez-Mendez et al. (LBL-7278, Dep. of Physics, Univ. of California, 1978).

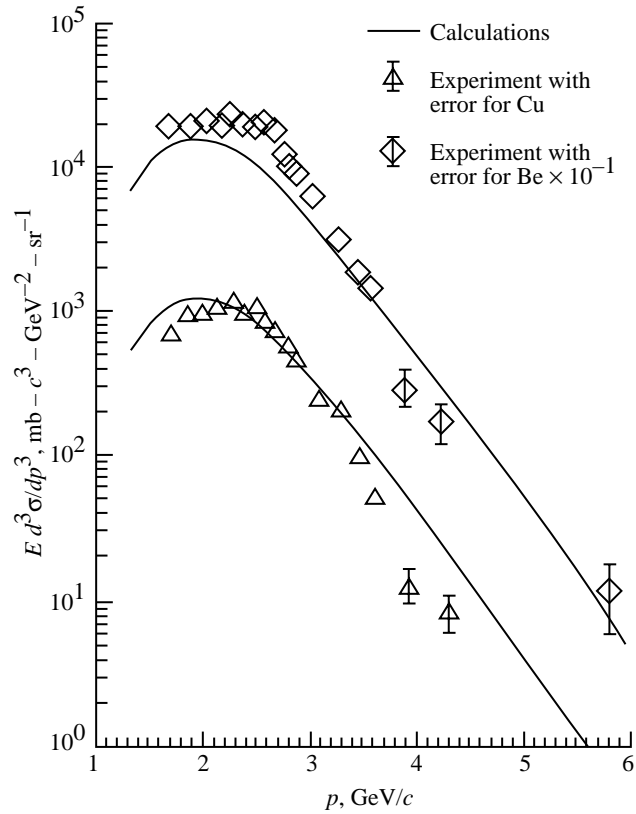


Figure 12. Comparison of proton production on $^{40}\text{Ar-Cu}$ and $^{40}\text{Ar-Be}$ collisions with production at 5° . Data are taken from reference 23 for 1.8A GeV beams.

Concluding Remarks

The production of nucleons from heavy ion abrasion has been formulated by using a multiple-scattering model. The resulting formalism allows for the physics of nuclear abrasion, which is important in describing heavy ion fragmentation cross sections to be directly related to the inclusive yields of nucleons. Comparisons of theory with experimental data were made for inclusive proton production at small angles, and good agreement was found. The model comparisons indicate an important role for final-state interaction effects and the internal momentum distribution of nucleons in describing nuclear fragmentation.

NASA Langley Research Center
 Hampton, VA 23681-0001
 August 25, 1994

Appendix

Kinematical Phase Space and Inclusive Momentum Distribution

In this appendix we discuss the relationship of the multiple production terms of nucleons abraded from the projectile to the kinematical phase space and also consider an approximation using the Glauber multiple-scattering series in which energy conservation is ignored entirely.

The scattering amplitude for the heavy ion collision is related to the cross section by the phase space of each particle that appears in the final state. We consider inclusive reactions in which a nucleon originating in the projectile is measured. For simplicity, the final target state is not considered and we use closure on these states with a single momentum vector denoted by \mathbf{p}_X to represent these states. The cross section is then determined by

$$d\sigma = \frac{(2\pi)^4}{\beta} \sum_X d\mathbf{p}_X d\mathbf{p}_{F^*} \sum_{n=1} \prod_{j=1}^n [d\mathbf{p}_j] \delta(E_i - E_f) \delta(\mathbf{p}_i - \mathbf{p}_f) |T_{fi}|^2 \quad (\text{A1})$$

where β is the relative projectile-target velocity, F^* represents the prefragments, n is the number of nucleons knocked out of the projectile in the overlap region with the target, and i and f denote the initial and final states, respectively. The prefragment will decay through particle emission if sufficient energy is available. To include the phase space of decay products of F^* , we write

$$d\mathbf{p}_{F^*} = d\mathbf{p}_F \prod_{r=0} d\mathbf{p}_r \quad (\text{A2})$$

where r denotes the ions (if any) emitted in ablation. In considering nucleon production from ablation, we would study \mathbf{p}_r . We use the momentum-conserving delta function in equation (A1) to eliminate \mathbf{p}_F from equation (A1).

We next consider using energy conservation in equation (A1). Working in the projectile rest frame, we transform $d\mathbf{p}_X$ to $d\mathbf{q}$, where $\mathbf{q} = \mathbf{p}_T - \mathbf{p}_X$ is the total momentum transfer in the collision, and we use the energy-conserving delta function in equation (A1) to eliminate dq_L , where q_L is the longitudinal momentum transfer. We then find

$$d\sigma = (2\pi)^4 \sum_X d\mathbf{q}_T K \left[\prod_{r=0} d\mathbf{p}_r \right] \left[\sum_{n=1} \prod_{j=1}^n d\mathbf{p}_j \right] |T_{fi}|^2 \quad (\text{A3})$$

where the phase space factor is defined as

$$K = \frac{1 - \partial E_f}{\beta \partial q_L} = \frac{1}{\beta} \frac{E_X E_{F^*}}{E_{F^*}(p_T - q_L) + E_X \left(\sum_j p_j \cos \theta_j - q_L \right)} \quad (\text{A4})$$

The momentum distribution of nucleons from abrasion is then

$$\frac{d\sigma}{d\mathbf{p}} = (2\pi)^4 \sum_X \int d\mathbf{q}_T \sum_{n=1} \int \prod_{j=2}^n d\mathbf{p}_j \prod_{r=0} d\mathbf{p}_r K |T_{fi}|^2 \quad (\text{A5})$$

which corresponds closely to equation (3) if we make the replacement

$$K = \int dq_L \delta(E_i - E_f) \rightarrow \int dE_{F^*} \delta(E_i - E_f) \quad (\text{A6})$$

If energy conservation is ignored entirely, we would have $K = 1$. By using the participant-spectator arrangement of the Glauber series discussed previously, the inclusive momentum distribution is shown to become

$$\frac{d\sigma}{d\mathbf{k}} = \sum_n \int d^2b \mathcal{P}^{A_P - n}(\mathbf{b}) \frac{dN_n}{d\mathbf{k}} \quad (\text{A7})$$

where

$$\frac{dN_n}{d\mathbf{k}} = \frac{dN_1}{d\mathbf{k}} [1 - \mathcal{P}(\mathbf{b})]^{n-1} \quad (\text{A8})$$

and

$$\int \frac{dN_1}{d\mathbf{k}} d\mathbf{k} = 1 - \mathcal{P}(\mathbf{b}) \quad (\text{A9})$$

The result of equation (A8) indicates that the inclusive momentum distribution from abrasion essentially follows the shape of the leading-order term in the approximations discussed because the absorptive factors in equation (A7) change slowly with increasing n for $A_P \gg 1$.

References

1. Wilson, John W.; Townsend, Lawrence W.; Schimmerling, Walter; Khandelwal, Govind S.; Khan, Ferdous; Nealy, John E.; Cucinotta, Francis A.; Simonsen, Lisa C.; Shinn, Judy L.; and Norbury, John W.: *Transport Methods and Interactions for Space Radiations*. NASA RP-1257, 1991.
2. Bowman, J. D.; Swiatecki, W. J.; and Tsang, C. F.: *Abrasion and Ablation of Heavy Ions*. LBL-2908, Univ. of California, July 1973.
3. Hüfner, J.; Schäfer, K.; and Schürmann, B.: Abrasion-Ablation in Reactions Between Relativistic Heavy Ions. *Phys. Rev. C*, vol. 12, no. 6, Dec. 1975, pp. 1888–1898.
4. Bleszynski, M.; and Sander, C.: Geometrical Aspects of High-Energy Peripheral Nucleus-Nucleus Collisions. *Nucl. Phys. A*, vol. 326, nos. 2–3, Sept. 10, 1979, pp. 525–535.
5. Townsend, L. W.; Wilson, J. W.; Cucinotta, F. A.; and Norbury, J. W.: Comparison of Abrasion Model Differences in Heavy Ion Fragmentation: Optical Versus Geometric Models. *Phys. Rev. C*, vol. 34, no. 4, Oct. 1986, pp. 1491–1494.
6. Cugnon, J.: Monte Carlo Calculation of High-Energy Heavy-Ion Interactions. *Phys. Rev. C*, vol. 22, no. 5, Nov. 1980, pp. 1885–1896.
7. Aichelin, Jörg: “Quantum” Molecular Dynamics—A Dynamical Microscopic n-Body Approach To Investigate Fragment Formation and the Nuclear Equation of State in Heavy Ion Collisions. *Phys. Rep.*, vol. 202, nos. 5–6, 1991, pp. 233–361.
8. Glauber, R. J.; and Matthiae, G.: High-Energy Scattering of Protons by Nuclei. *Nucl. Phys.*, vol. B21, no. 1, Aug. 1, 1970, pp. 135–157.
9. Czyz, W.; and Maximon, L. C.: High Energy, Small Angle Elastic Scattering of Strongly Interacting Composite Particles. *Ann. Phys. (N.Y.)*, vol. 52, no. 1, Mar. 1969, pp. 59–121.
10. Cucinotta, Francis A.; Townsend, Lawrence W.; and Wilson, John W.: Multiple-Scattering Effects in Quasi-elastic α - ^4He Scattering. *Phys. Rev. C*, vol. 46, no. 4, Oct. 1992, pp. 1451–1456.
11. Cucinotta, Francis A.; and Dubey, Rajendra R.: *Final State Interactions and Inclusive Nuclear Collisions*. NASA TP-3353, 1993.
12. Hatch, R. L.; and Koonin, S. E.: High Momentum Nucleons From Relativistic Nuclear Collisions. *Phys. Lett.*, vol. 81B, no. 1, Jan. 29, 1979, pp. 1–4.
13. Cucinotta, Francis A.; Townsend, Lawrence W.; and Wilson, John W.: Inclusive Inelastic Scattering of Heavy Ions in the Independent Particle Model. *J. Phys. G: Nucl. Particle Phys.*, vol. 18, no. 5, May 1992, pp. 889–901.
14. Antonov, A. N.; Hodgson, P. E.; and Petkov, I. Zh.: *Nucleon Momentum and Density Distributions in Nuclei*. Oxford Univ. Press, 1988.
15. Frankel, Sherman: Basis for Quasi-Two-Body Scaling. *Phys. Rev. C*, vol. 17, no. 2, Feb. 1978, pp. 694–701.
16. Amado, R. D.; and Woloshyn, R. M.: Mechanism for 180° Proton Production in Energetic Proton-Nucleus Collisions. *Phys. Rev. Lett.*, vol. 36, no. 24, June 1976, pp. 1435–1437.
17. Haneishi, Y.; and Fujita, T.: Problem of Backward Proton Production. *Phys. Rev. C*, vol. 33, no. 1, Jan. 1986, pp. 260–274.
18. Moniz, E. J.; Sick, I.; Whitney, R. R.; Ficenece, J. R.; Kephart, R. D.; and Trower, W. P.: Nuclear Fermi Momenta From Quasielastic Electron Scattering. *Phys. Rev. Lett.*, vol. 26, no. 8, Feb. 22, 1971, pp. 445–448.
19. Amado, R. D.: Momentum Distributions in the Nucleus. *Phys. Rev. C*, vol. 14, no. 3, Sept. 1976, pp. 1264–1270.
20. Anderson, L.; Brückner, W.; Moeller, E.; Nagamiya, S.; Nissen-Meyer, S.; Schroeder, L.; Shapiro, G.; and Steiner, H.: Inclusive Particle Production at Forward Angles From Collisions of Light Relativistic Nuclei: Nuclear Fragments. *Phys. Rev. C*, vol. 28, no. 3, Sept. 1983, pp. 1224–1245.
21. Anderson, L.; Moeller, E.; Nagamiya, S.; Nissen-Meyer, S.; Schroeder, L.; Shapiro, G.; and Steiner, H.: *Inclusive Particle Production at Forward Angles From Collisions of Light Relativistic Nuclei, Part III: Data Tables*. LBL-14330, Dep. of Physics, Univ. of California, May 1982.
22. Nagamiya, S.; Anderson, L.; Brückner, W.; Chamberlain, O.; Lemaire, M.-C.; Schnetzer, S.; Shapiro, G.; Steiner, H.; and Tanihata, I.: Wide-Angle High-Energy Proton Spectra by 800 MeV/A C, Ne, and Ar Beams. *Phys. Lett.*, vol. 81B, no. 2, Feb. 12, 1979, pp. 147–150.
23. Gosset, J.; Kapusta, J. I.; and Westfall, G. D.: Calculations With the Nuclear Firestreak Model. *Phys. Rev. C*, vol. 18, no. 2, Aug. 1978, pp. 844–855.

REPORT DOCUMENTATION PAGE			Form Approved OMB No. 0704-0188	
Public reporting burden for this collection of information is estimated to average 1 hour per response, including the time for reviewing instructions, searching existing data sources, gathering and maintaining the data needed, and completing and reviewing the collection of information. Send comments regarding this burden estimate or any other aspect of this collection of information, including suggestions for reducing this burden, to Washington Headquarters Services, Directorate for Information Operations and Reports, 1215 Jefferson Davis Highway, Suite 1204, Arlington, VA 22202-4302, and to the Office of Management and Budget, Paperwork Reduction Project (0704-0188), Washington, DC 20503.				
1. AGENCY USE ONLY (Leave blank)	2. REPORT DATE November 1994	3. REPORT TYPE AND DATES COVERED Technical Paper		
4. TITLE AND SUBTITLE Multiple-Scattering Model for Inclusive Proton Production in Heavy Ion Collisions			5. FUNDING NUMBERS WU 199-45-16-11	
6. AUTHOR(S) Francis A. Cucinotta				
7. PERFORMING ORGANIZATION NAME(S) AND ADDRESS(ES) NASA Langley Research Center Hampton, VA 23681-0001			8. PERFORMING ORGANIZATION REPORT NUMBER L-17387	
9. SPONSORING/MONITORING AGENCY NAME(S) AND ADDRESS(ES) National Aeronautics and Space Administration Washington, DC 20546-0001			10. SPONSORING/MONITORING AGENCY REPORT NUMBER NASA TP-3470	
11. SUPPLEMENTARY NOTES				
12a. DISTRIBUTION/AVAILABILITY STATEMENT Unclassified-Unlimited Subject Category 73			12b. DISTRIBUTION CODE	
13. ABSTRACT (Maximum 200 words) A formalism is developed for evaluating the momentum distribution for proton production in nuclear abrasion during heavy ion collisions using the Glauber multiple-scattering series. Several models for the one-body density matrix of nuclei are considered for performing numerical calculations. Calculations for the momentum distribution of protons in abrasion are compared with experimental data for inclusive proton production.				
14. SUBJECT TERMS Nuclear fragmentation; Heavy ions; Proton production; Galactic cosmic radiation			15. NUMBER OF PAGES 18	
			16. PRICE CODE A03	
17. SECURITY CLASSIFICATION OF REPORT Unclassified	18. SECURITY CLASSIFICATION OF THIS PAGE Unclassified	19. SECURITY CLASSIFICATION OF ABSTRACT Unclassified	20. LIMITATION OF ABSTRACT	